Student thesis series INES nr 625

Seasonal variation of LAI in Swedish coniferous forest

Ilia Mastepanov

2023
Department of
Physical Geography and Ecosystem Science
Lund University
Sölvegatan 12
S-223 62 Lund
Sweden

Ilia Mastepanov (2023).
Seasonal variation of LAI in Swedish coniferous forest
Säsongsvariation av LAI i svensk barrskog
Bachelor degree thesis, 15 credits in Physical Geography and Ecosystem Analysis
Department of Physical Geography and Ecosystem Science, Lund University

Level: Bachelor of Science (BSc)

Course duration: *March* 2023 until *June* 2023

Disclaimer

Seasonal variation of LAI in Swedish coniferous forest

Ilia Mastepanov

Bachelor thesis, 15 credits, in Physical Geography and Ecosystem Analysis

Thomas Holst
Researcher, Dept of Physical Geography and Ecosystem Science

Exam committee:
Karin Larsson, Lecturer, Dept of Physical Geography and Ecosystem Science
Anna Terskaia, Researcher, Dept of Physical Geography and Ecosystem Science

Acknowledgements

Thanks to my supervisor, Thomas Holst for guiding me during the course of writing this thesis, and ICOS Hyltemossa station for providing the data on radiation and manual LAI measurements.

Abstract

Leaf Area Index (LAI) is quantity representing the amount of foliage in the canopy, which makes it an important parameter for analysing terrestrial ecosystems. Traditional methods of measuring LAI were done by analysing hemispherical photographs by hand and were very time consuming, requiring specific weather conditions (Jonckheere et al. 2004). Modern methods, including remote sensing, have much higher automation, yielding continuous data. In this thesis, LAI for a spruce forest at Hyltemossa ICOS site was calculated and plotted as a continous time series, and the results were compared to available discontinuous measurements done using hemispherical photographs, as well as other studies of LAI for coniferous forests. The resulting values showed no seasonal or multiannual trend, but generally match the findings of several other studies, with the obtained values between 4 and 5 being typical for coniferous forest (Parker 2020).

Table of Contents

1 Introduction

Modern science has advanced very far in the field of remote sensing. Current methods allow for collection and processing of enormous amounts of data. On the other hand, there is the classic scientific approach, with much smaller data collection capabilities, but much deeper understanding of what is being collected. Combining the best of both approaches could only happen with a variable that has been both sampled manually with the classical approach for many years with high understanding on what it is and how it affects other variables and processes, while at the same time being something that could be sampled through remote sensing for large periods of time. One example of such a variable is Leaf Area Index (LAI).

1.1 Study aim

The aim of this study is to assess LAI on a continuous basis using continuous Photosynthetically Active Radiation (PAR) measurements for the ICOS site at Hyltemossa.

This can be achieved by answering several research questions:

- How does the extinction coefficient k vary for different weather conditions throughout the seasons?
- Is the calculated LAI in the same range as the measured discontinuous values?
- Is it possible to detect and quantify changes in LAI during times of plant stress such as drought or intense snowfall?

2 Background.

Leaf Area Index (LAI) is a quantity typically defined as the one-sided leaf area per unit ground area (Watson 1952) This was later refined as the one-sided projected leaf area (Ross 1981). For conifers or other trees with non-flat leaves, an updated definition is used, that being half of the interception area per unit ground area (Chen and Black 1992), this is the definition that will be used in this thesis. Some studies use $m^2 * m^{-2}$ as a unit for LAI (Mencuccini and Bonosi 2001) however it is also common to see it defined as dimensionless and unitless (Nassar et al. 2020), (Bendavid et al. 2023) and this definition will be used in this thesis.

Since LAI is a representation of the leaf area in the canopy it is an important parameter for several ecological, hydrological, and biogeochemical processes, as explained in Advanced Remote Sensing (second edition) (Liang and Wang 2020). LAI can be used to estimate

photosynthetic rate and primary production, making it an important parameter for ecosystem analysis (Parker 2020).

LAI can be measured in several ways. The most common traditional method is hemispherical canopy photography as described by Hutchinson and Matt (1977), which involves taking a fisheye photograph of the canopy and then manually calculating how much of its area is covered by the canopy itself and how much is taken up by the sky. The process is rather time consuming and relies on suitable weather conditions where the sky is homogenous, clear and overcast conditions are preferable, with overcast being the better of the two since there in less reflections from the leaves. Another method is using litter traps to collect fallen leaves, but this can only be done during the autumn leaf fall period (Jonckheere et al. 2004). The same method can be used all year round for coniferous forests (Wang et al. 2017). There is also the destructive method which involves the total removal of all biomass from the sample (Jonckheere et al. 2004), but this is very rarely used for coniferous forest as it is very labour intensive for larger samples and results in the destruction of the trees. An indirect method incorporates the use of remote sensing and satellite data as described by Chen and Cihlar (1996). This involves analysing satellite or aerial images and identifying what part of the study area is taken up by the tree canopies. This method is becoming more widespread as higher resolutions become available for use, and more studies chose this method for data collection, both using satellite imagery (Hojas Gascón et al. 2019) as well as aerial photography (Li et al. 2018).

Despite the fact that LAI was primarily developed for use in deciduous forest (Hutchison and Matt 1977), many studies have been done on coniferous forest as well, (Chen et al. 1997; Thimonier et al. 2010; Qu et al. 2017). During the last decade, several studies focused on obtaining a continuous LAI time series (Ryu et al. 2012; Gonsamo and Chen 2014; Yan et al. 2019).

3 Methods.

3.1 Study site

Hyltemossa ICOS (Integrated Carbon Observation System) site, which is located in northwestern Scania (56°06′N, 13°25′E) was chosen. The site is a coniferous forest dominated by Norway Spruce (*Picea abies*). The site is a managed forest with a management turnover of 50 years (ICOS-Sweden 2023). The last clear cutting happened in 1982 and the forest was replanted a year later. It was last thinned in 2013 (ICOS-Sweden 2023). The average tree density is 611 trees per hectare, with an average tree height of 19 metres. The main tower on

the site, carrying most of the radiation sensors, reaches above the canopy. The continuous incoming photosynthetically active radiation (PAR) is measured at the top, at a height of 150 metres. This includes both the total and the diffuse part. The site has a total of 20 radiation sensors located under the canopy at a height of 1.3 metres above the surface, split into 4 Continuous Plots (CPs) of 5 sensors each. An average of all 20 is used, as to minimise the effects of noise. This site was chosen as it has all the necessary data readily available, both continuous and discontinuous spanning all the way back to 2018, meaning that it will be easy to get several years of LAI.

Figure 1. Aerial view of the site at Hyltemossa. Relevant points of interest for this thesis are the main tower (marked in red) and the four continuous plots (CP). Also included are the spatial sampling plots (SP-I) and the boundaries of the two forest stands, stand characteristics in stand A differ in terms of tree height, density and DBH from characteristics in stand B (Image source – https://www.icos-sweden.se/hyltemossa ICOS RI, licensed under CC4BY)

3.2 Data used

The data used comes from the ICOS ETC Meteosens dataset, which contains half-hourly meteorological variables for different sensors installed at the site. The first data series is the Near Real Time file ICOSETC_SE-Htm_METEOSENS_NRT (Heliasz et al. 2023) which starts in Sepmtember 2022 and ends in April 2023. This file is updated once a day, meaning

that the delay between measurement and publication should be maximum 24 hours. The second data series is the Level 2 file ICOSETC_SE-Htm_METEOSENS_INTERIM_L2 (Heliasz et al. 2022) which covers the time from the start of 2018 up to where the NRT file starts. The main point of interest here are the following columns: PPFD_IN_1_1_1 which is the above-canopy incoming radiation (where PPFD stands for photosynthetic photon flux density, a measure of PAR), PPFD_DIF_1_1_1 which is the diffuse part of the incoming radiation, and the twenty PPFD_BC columns which are the below-canopy radiation sensors. The rest of the information in these files was not used in this thesis. Care was taken to remove instances of missing data, which meant that some of the BC sensors were ultimately deleted as they were not showing data, but noise consisting of virtually zero values (±0.1 μmol/m^2s). Unfortunately, the Level 2 dataset lacked a lot of the required data, namely the below-canopy radiation before 2021, and so six other files were used for that. These included the SE-Htm_meteo_2018_CP_flag file and the SE-Htm_eco_2018_CP_flag file, as well as their respective versions for 2019 and 2020 (Biermann et al. 2020a, b; Biermann et al. 2020c, d; Biermann et al. 2021a, b). Still, the complete data series has several large gaps in it, caused by the instruments being turned off, either for maintenance or due to malfunction. The largest ones are July-August 2022, September2019-December 2020 and October2020-August 2021. Gaps of several hours or even a few days were more common, but they do not affect the results nearly as much.

Several discontinuous values of LAI are available for the years 2018- 2022 (ICOS-Sweden 2023). These represent the mean LAI for that month and are based on at least seven quality controlled Digital Hemispherical Photographs (DHP) taken in each of four CPs during that month.

3.3 Calculations

LAI can be calculated using the following formula, a rewritten form of Beer's law, taken from (Holst et al. 2004):

$$LAI = (-1/k) * \ln(PAR/PAR_0)$$

Equation 1.

Where **k** is the extinction coefficient representing how well light passes through a medium, **PAR** is the Photosynthetically Active Radiation measured below the canopy and $\mathbf{PAR_0}$ is the radiation measured above the trees.

Only the PAR values measured from 10:00 to 14:00 (local time, CET) for each day was used. The source data had different timestamps (UTC or CET) and care was taken to convert all the data to a CET timestamp. For Hyltemossa, geographical noon is almost 12:00 CET, so the data interval of two hours before and after noon was chosen. This was done as that time is when the incoming radiation reaches its peak and the sunlight falls onto the canopy at the highest angle, reducing the effect of noise on the data.

3.3.1 Extinction coefficient calculations

PAR and $\mathbf{PAR_0}$ are readily available from the data, while **k** needs to be calculated. This can be done by reversing equation 1 and using the existing measured LAI values. Extinction coefficient **k** is dependent on how sunlight is scattered in the canopy which changes with the ratio of direct and diffuse radiation. Since this depends on the atmospheric conditions, particularly cloud cover, a method to classify the conditions was formulated. This requires calculating the direct incoming radiation, which is done by subtracting the diffuse part from the total radiation. With the help of a model, potential PAR was calculated based on potential solar flux, modelled using formulae from Kalogirou (2012). The model calculates potential PAR using latitude, day of year and time of day. Using the model, potential PAR values were calculated for the whole year in 30-minute resolution. From there, the ratio of measured direct PAR to potential PAR was calculated for every data point and separated into three categories with the following thresholds: clear (> 0.8), cloudy (0.4-0.8) and overcast (< 0.4). The thresholds were taken from Holst et al. (2004).
For every month that had a measured LAI value, three values of k were calculated, one for each weather category (clear, cloudy, overcast). The value of k was calculated for every 30-minute data point and then a mean value for the month was taken. Not all months have a measured LAI value, for the months without a measured LAI, the k values were taken assumed to be identical to the closest month that has a LAI measured, meaning that on average, two or three months in a row are using the same values of k.

4 Results.

The first step was to determine if a seasonal pattern exists based on the measured LAI values (ICOS-Sweden 2023). Figure 2 shows all the values of LAI for the five years of measurements and their standard deviation as vertical error bars.

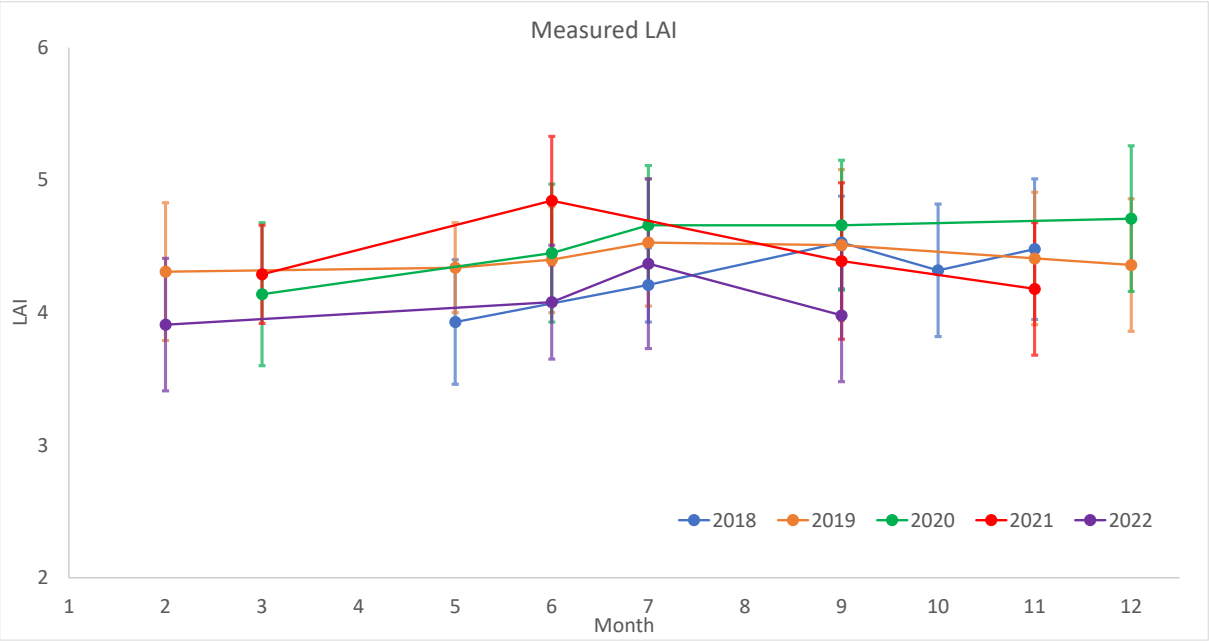

Figure 2. Seasonal variation of the mean monthly LAI values measured by ICOS. Error bars represent standard deviation.

The values of LAI varied from 3.9 to 4.8, while the standard deviation had a mean value of 0.48. During the first half of the year, LAI seems to increase, during the second half it is mostly decreasing. Given the magnitude of the standard deviation (size of the error bars), it is impossible to say whether the apparent variation in individual LAI values, both between the different seasons and between the different years, is due to actual seasonal patterns or interannual variations, or simply an uncertainty of the values.

In order to determine the yearly variation of incoming PAR, the data for 2018 was chosen, as it is the most complete out of all years with no major breaks in the data. The data is plotted in Figure 3.

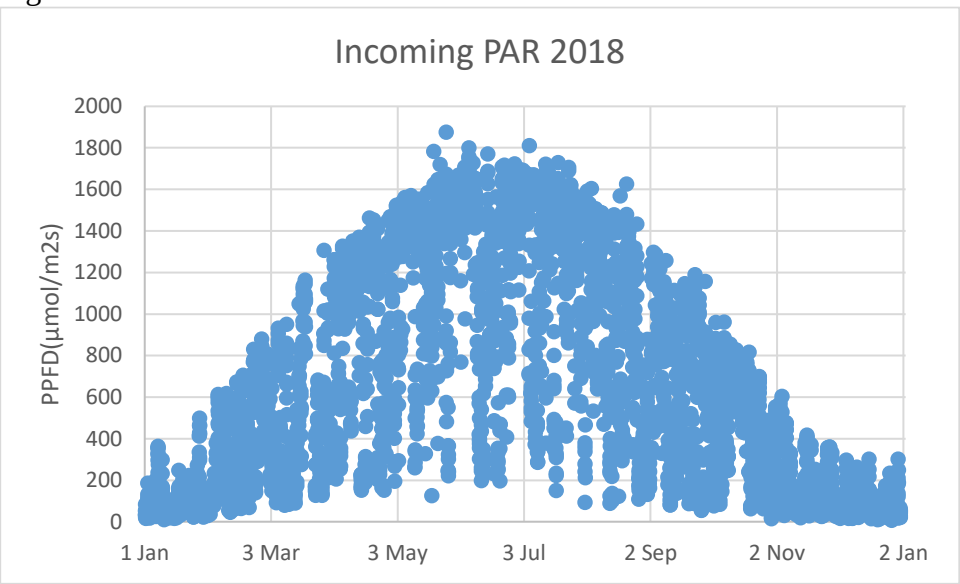

Figure 3. Yearly pattern of incoming PAR for 2018 for the time of day from 10:00 to 14:00

The graph shows all quality-controlled individual readings of PAR in 2018 within the time from10:00 to 14:00 every day. The upper boundary of the point cloud represents the incoming radiation on the sunny days, while the lower boundary represents the overcast days. The data shows that overcast weather was quite often, but the individual measurements from days with clear weather can be found throughout the whole year.

To assess correspondence between the PAR readings on the most sunny days and the potential PAR obtained with the model, four days were selected from different seasons which were the least cloudy (January 27th, April 2nd, July 2nd, October 15th). The measured and modelled PAR values for these days are plotted in Figure 4. Ratios between measured and modelled PAR are shown in Figure 5.

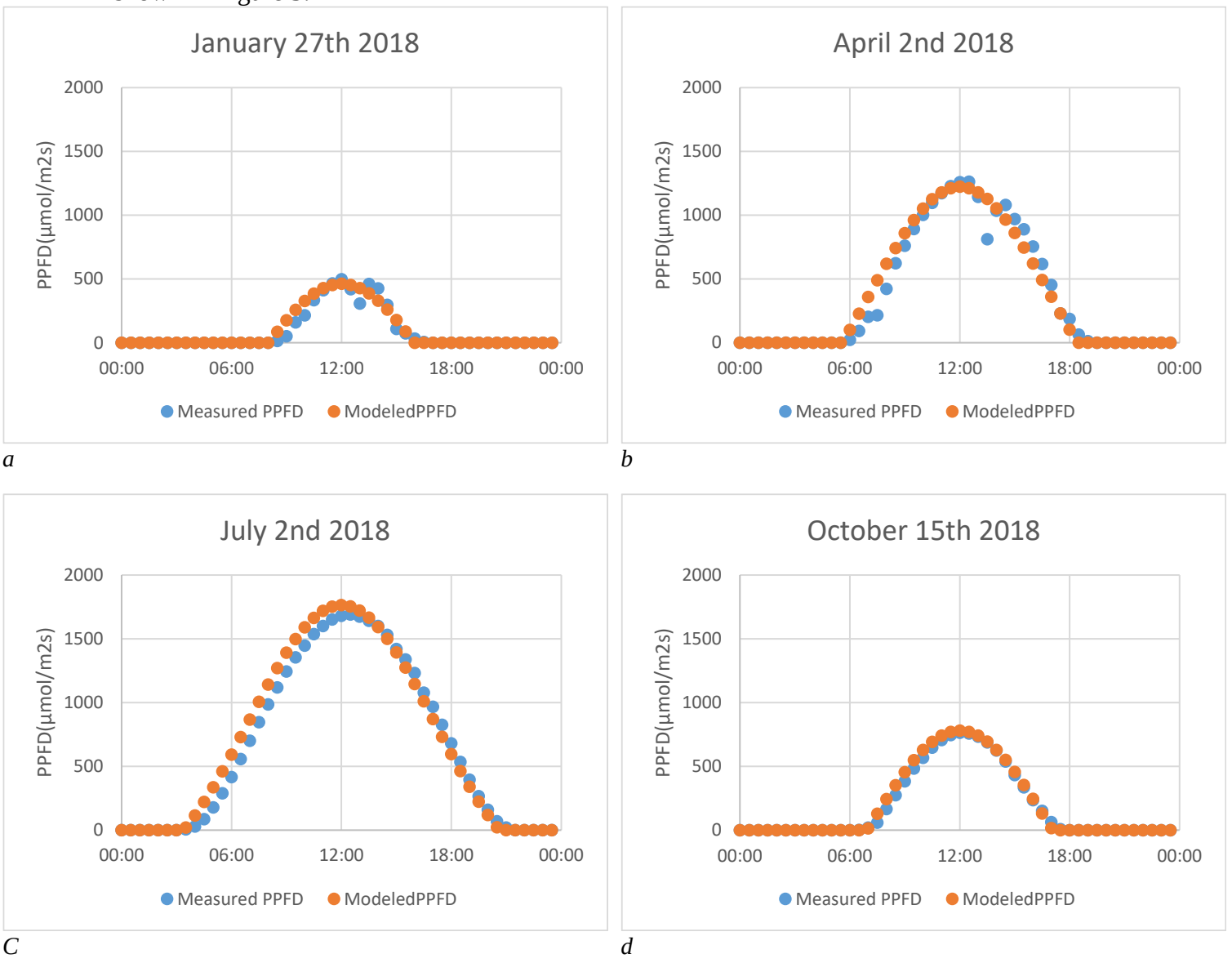

Figure 4. Comparison of modelled potential PAR and measured incoming PAR for selected days from different seasons 2018.

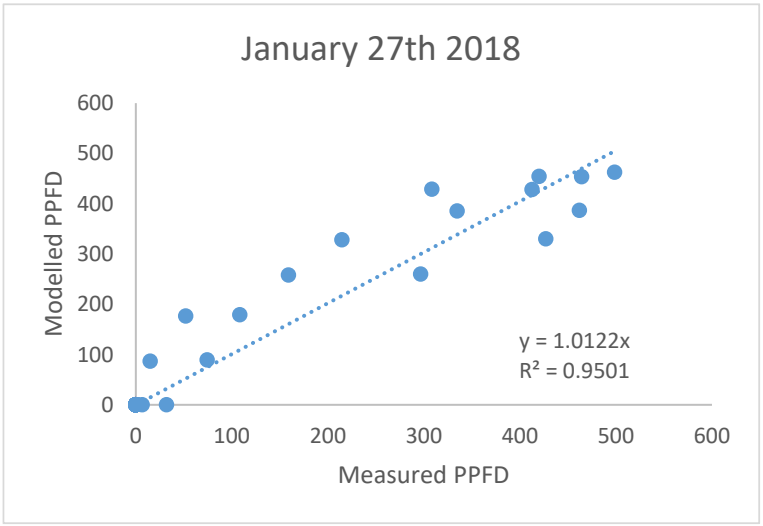

a

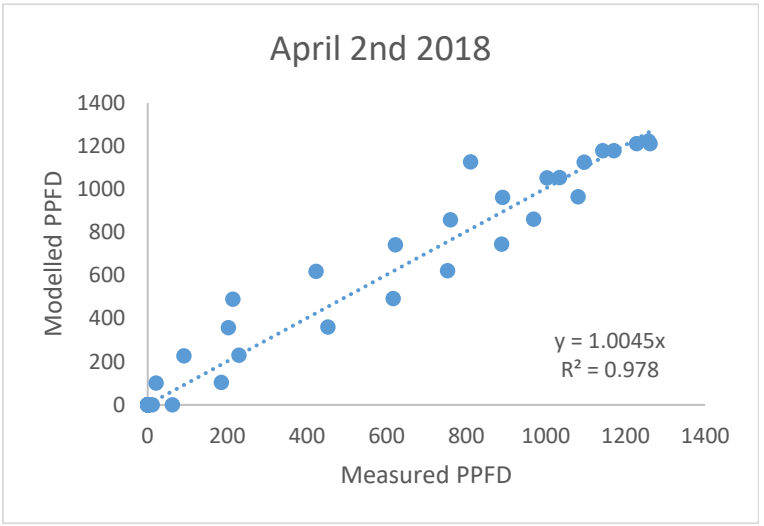

b

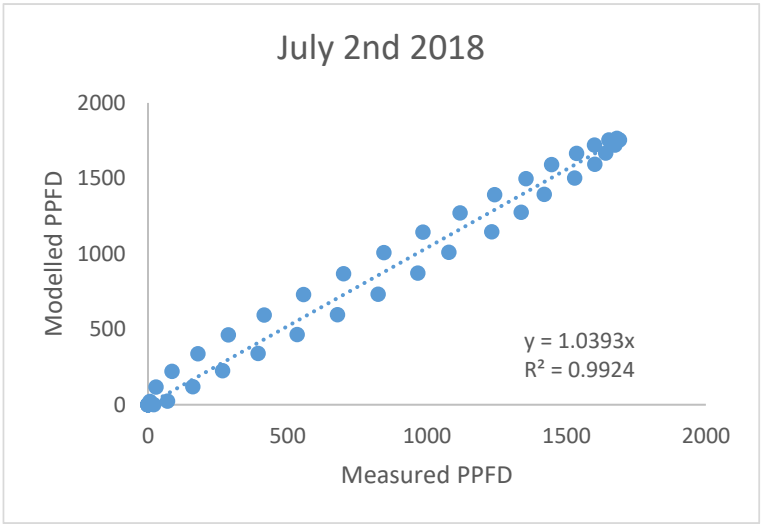

c

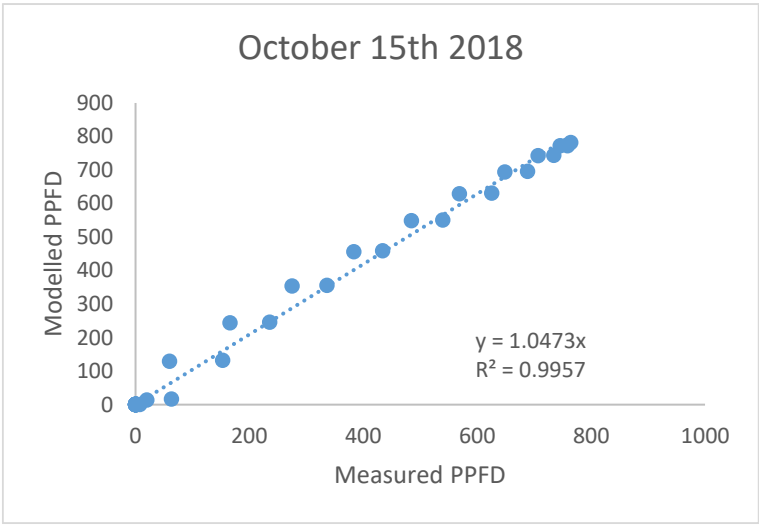

d

Figure 5. Scatter plots for ratios measured/modelled PPFD for selected days from different seasons 2018.

The modelled values correspond well with the measured values, especially in summer. For each of the four days, the ratio is close to one, R^2 between 0.95 and 0.996. For July 2nd, the hysteresis between morning and evening can be clearly seen. This can be caused by a mismatch in time between the two data series. Overall, the difference between measured and modelled PAR was considered insignificant.

As a measure of the trees' efficiency in intercepting PAR, the ratio between below-canopy PAR and incoming PAR was used (Figure 6). The original data contained one month (September) with ratio close to 1, which is highly unrealistic, so the month was excluded from Figure 6. The original data is plotted on Figure S1.

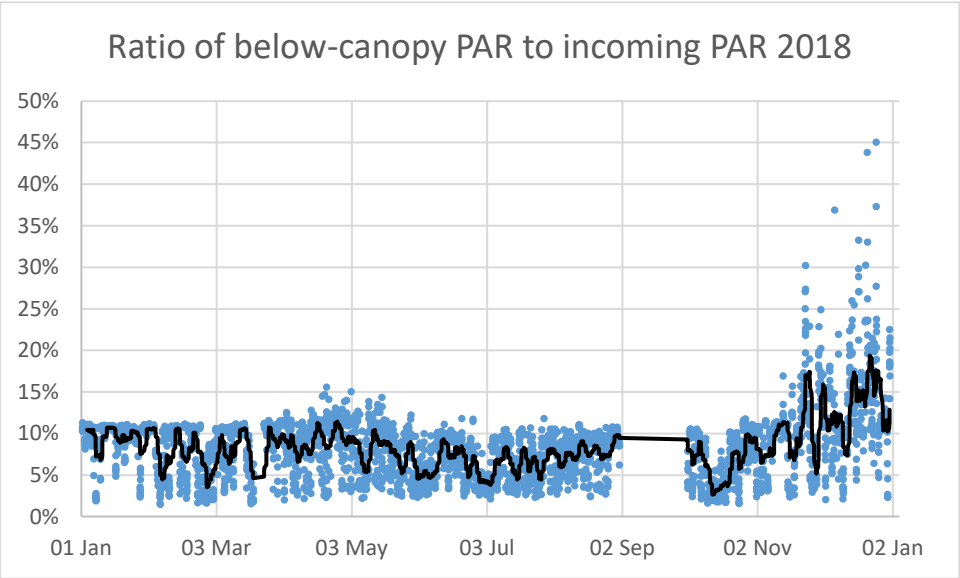

Figure 6. Ratio of below-canopy PAR to incoming PAR. Blue dots: individual values, black line: moving average over three days. September excluded.

Most values are lying in the interval 5%-10% with some reaching as far as 45% at the end of the year. Thus 90% - 95% of the incoming PAR is intercepted by the canopy. The fact that the understorey vegetation in Hyltemossa is rather sparse and mostly consists of mosses (ICOS-Sweden 2023), tells that this level of PAR interception is typical for this forest at least for several decades.

Extinction coefficient k values for clear weather during each month were plotted in Figure 7. Similar graphs for cloudy and overcast weather are presented in supplementary materials (Figure S2 and S3).

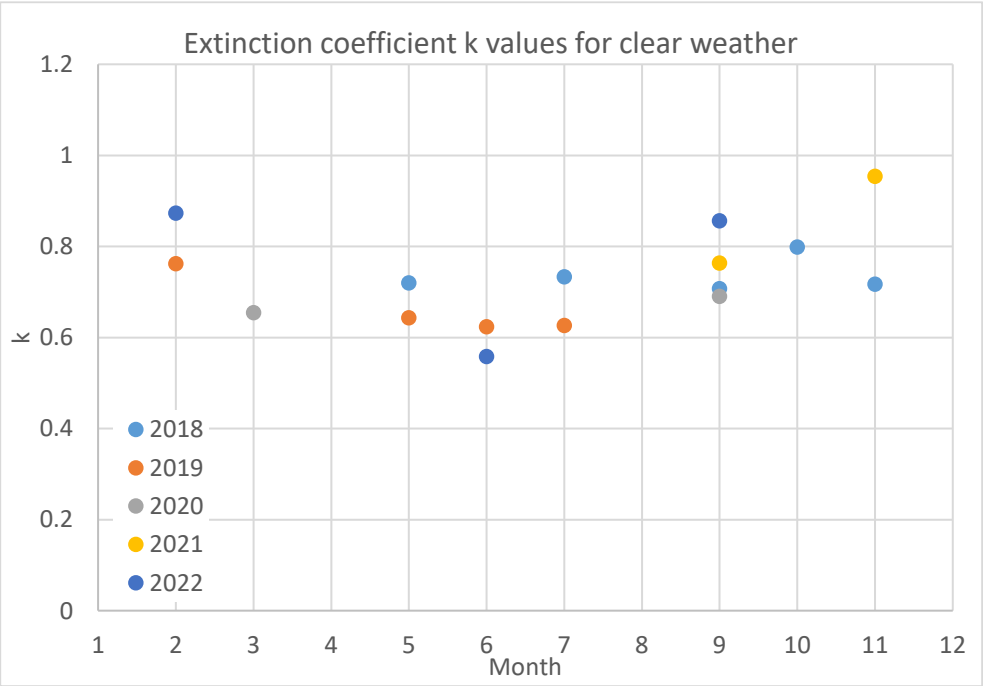

Figure 7. Values of k (extinction coefficient) for clear weather each month of measurement 2018-2022.

Including all three weather categories, values of k vary from 0.46 to 0.95 with a mean value of 0.64. For clear weather, k decreases from January to June and then increases again from June to December. The other categories do not show such a clear pattern, but during the summer months, the spread is less than other seasons.

Calculated values of LAI for 2018-2022 are presented on Figure 8.

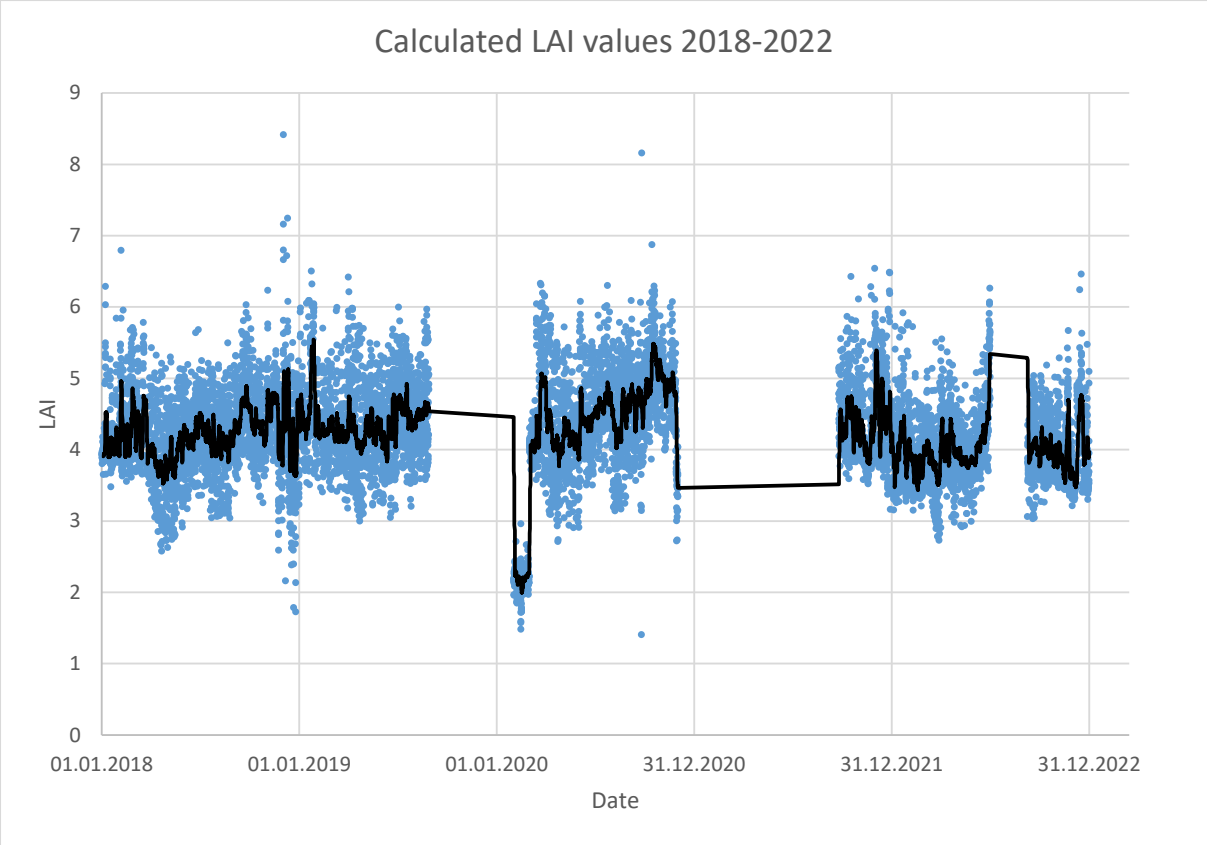

Figure 8. Calculated values of LAI for the entire five-year period. Blue dots: individual 30-min values during 10:00 – 14:00, black line: moving average over three days.

The majority of LAI values are in the range 3 - 6. When taking the moving average over the period of three days, the LAI values are around 4-5. There is no clear seasonality in the data, and there is no clear multiannual trend.

Similar Figures S4-S6 (supplementary materials) show the plotted LAI values separated by the three different weather categories. The spread of values appears larger for clear weather (Figure S4) and smaller for overcast weather (Figure S6).

The same data overlayed with the LAI values measured by ICOS-Sweden (2023) is presented on Figure 9.

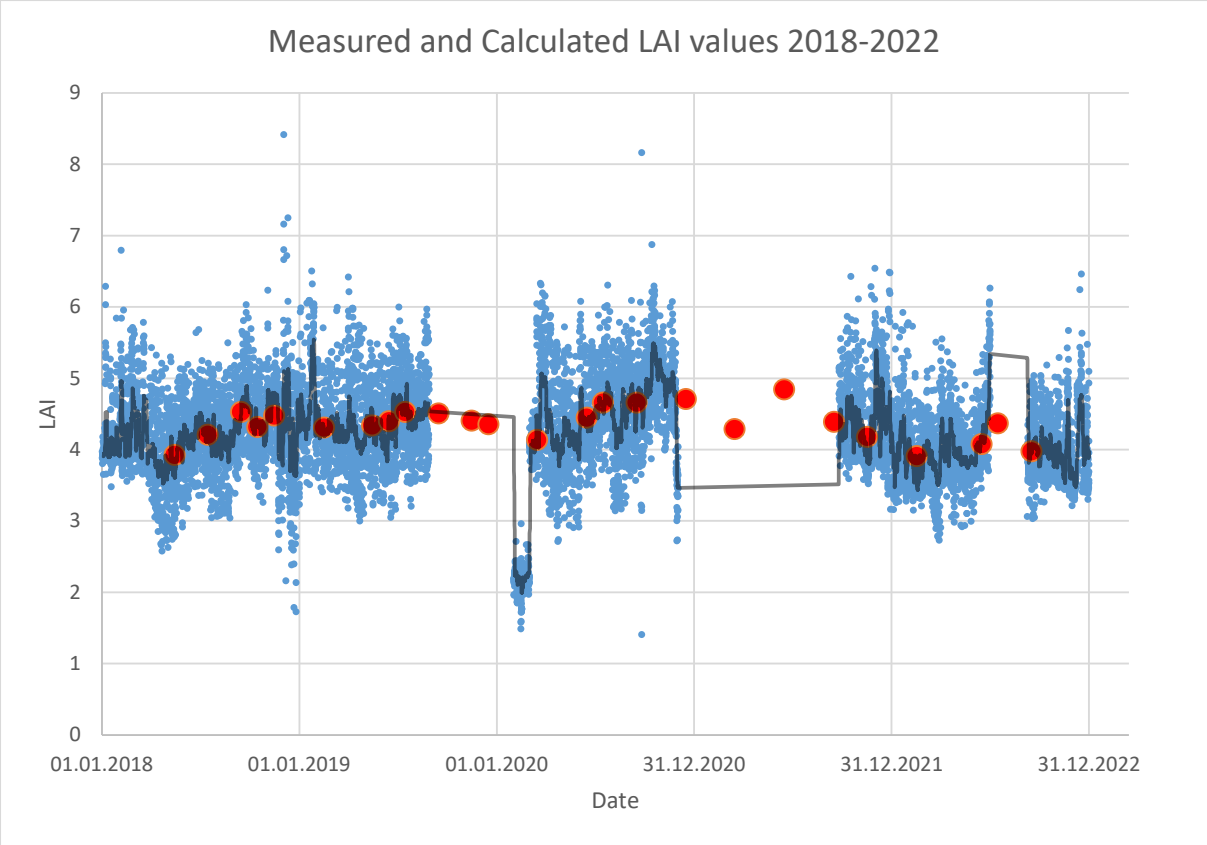

Figure 9. Measured and calculated values of LAI for the entire five-year period. Red dots: measured LAI values, blue dots: individual calculated 30-min values during 10:00 – 14:00, black line: moving average over three days of calculated LAI.

The calculated values, especially their averages, match the pattern of the measured LAI very closely.

5 Discussion.

Since Hyltemossa is a coniferous forest, no very large seasonal changes in LAI were expected (Wang et al. 2017). The data has a high standard deviation which hides potential small changes in LAI. The high standard deviation comes from the fact that every LAI value was a mean from at least seven measurements in each of the four CPs, and the standard deviation reflects both the spatial variation between the CPs and the temporal variation between the measurements.

When looking at Figure 4, there is a difference between when the modelled PAR begins to increase, and when the actual PAR begins to increase. Looking at the data, it would appear that the actual PAR starts to increase about half an hour after the modelled. This is most likely the case because of different conventions of timestamps in the data and in the model. The model apparently considers PAR at the exact stated moment in time, i.e., 10:00. The actual

PAR is measured every 5 seconds, then averaged over thirty minutes. The SE-Htm_meteo_20xx_CP_flag file and the SE-Htm_eco_20xx_CP_flag series of files, that were used for Figure 4, only have one time stated, and it is not clear whether this is the start or end of the thirty-minute interval. If it is the start time, then it would be better to model PAR fifteen minutes later; if it is the end time, then fifteen minutes earlier. Thus, a small shift in time between modelled and measured PAR can be expected, but on a scale larger than several hours this is not significant.

In Figure 6, we do not see any clear trend between January and August. From October to December, there is an increase in the ratio of below-canopy PAR to incoming PAR, from 5%-10% to 10%-15% (average over three days). This could indicate a loss of needles due to strong winds during autumn, but no clear drop in LAI is seen during these months (Figure 8). During September, the ratio was very close to 100%, (Figure S1) meaning that the radiation above and below the trees is almost identical, which is only possible if there is nothing above the sensor. This is highly unlikely, considering that this is the average value from all below-canopy sensors which are spread across four CPs. Most likely this an error, possibly caused by instrument calibration or the like, as this data anomaly lasts for exactly the whole month, starting exactly September 1st and goes back to realistic values on October 1st.

The values of k plotted on Figure 7, show a decrease during summer. This is most likely caused by a higher sun angle. Because the radiation on clear days is mostly direct, the sun angle has an effect on how much of the canopy the sunlight has to go though. During the summer, sunlight falls at a higher angle and its path through the canopy is shortest, meaning that more sunlight reaches the ground. During the winter when the angle is at its flattest, the sunlight's path through the canopy is longer, and less sunlight reaches the ground. In cloudy and overcast weather condition, diffuse radiation comprises a larger share of the total radiation, meaning that the effect of sun angle is less important. When considering the five years, the values of k for the specific months are not far apart and most likely no significant loss of accuracy were to take place if one was to substitute them. In theory, calculating LAI for other years with some variation of these values is possible, going further into the past as well as looking into the future. However, the three separate values of k are still needed as the difference between them is substantial.

The calculated LAI values shown in Figure 9 were very close to the measured ones, but there were some areas that were significantly off, for instance the start of 2020. This is most likely an error with the data, supported by the fact that it is directly after a large gap in the data. A possible explanation is that the instrument was not calibrated properly after a malfunction or replacement/maintenance. I am unsure if I can dismiss this data.

Because no clear pattern is visible in the distribution of calculated LAI, it is hard to tell whether drops in LAI are caused by a loss of needles due to plant stress, such as during a drought or extreme snowfall. During the five years of measurements, several of these events have occurred, but it is impossible to identify them on the graph.

One thing that was not considered in the method was the fact that 2020 was a leap year and 2018, 2019, 2021 and 2022 were not. The model of potential PAR does not consider differences between calendar and astronomic years. A normal calendar year is about six hours shorter than an astronomic year, and a leap calendar year is about eighteen hours longer than an astronomic year. The model simply divides the year into 365 days. Thus, a very high degree of accuracy with the model is not possible. However, a larger uncertainty can be caused by variability in atmospheric turbulence, particle concentration and humidity, so the adjustment in time was not considered important.

Comparing the LAI values obtained with the results from other studies, Chen and Cihlar (1996) measured LAI values of around 3-4 for black spruce (*Picea mariana*) near Thompson, Manitoba. Curiously, the site is on a similar latitude to Hyltemossa (55.74N for Thompson, 56.1N for Hyltemossa), meaning that the incoming radiation is very similar, and that the LAI values can be compared fairly. The LAI values obtained are similar enough to the average values for Hyltemossa, the differences can most likely be attributed to the different species of spruce and a different forest density. The data from Chen and Cihlar was also collected only during late spring of one specific year, which is another reason as to the differences in resulting LAI.

Another study by Mencuccini and Bonosi (2001) measured LAI for Scots pine (*Pinus sylvestris*) for five study sites, three in Italy, one in Finland and one in the UK. The LAI was measured for a period of several months during various years from 1992-1996 and varied from 2.0- 3.8. The values are considerably lower than the average ones for Hyltemossa (4-5), however this is likely due to the different species of conifer. Interestingly, the forest density for the sites is higher than in Hyltemossa (around 1600 trees per hectare, compared to around 600) and yet the LAI is smaller. Perhaps pine forest has naturally lower LAI value than spruce.

The seasonal variation in LAI for deciduous forest were measured by Qiao et al. (2019) for several sites in the US, Canada, and Japan. The LAI showed a clear seasonal trend, being zero during the winter then increasing rapidly to reach a maximum of around 4 to 5 during the

summer, before quickly falling back to zero. The change is very drastic and happens over the course of a few months.

For conifers the yearly variation is much less. In a study by Wang et al. (2017) yearly LAI distribution was measured for two sites in Canada with eastern white pine forest (*Pinus strobus*) as well as three sites in China with a mixed evergreen-decidious forest consisting of Korean pine (*Pinus koraiensis*) and a mix of spruce and fir (*Abies nephrolepis* and *Picea* spp.). LAI was collected many times per year, and a seasonal variation was established. The changes are less drastic compared to a deciduous forest, but they are present, with a clear increase and a peak of up to 8 or 6 during summer, and then a decrease leading into the winter with a minimum of around 4. Quite large standard deviation is present, maximum of around 2 on some measurements, but they do not obscure the seasonal LAI pattern. The measured LAI values for Hyltemossa are unfortunately less frequent, and so seasonal patterns are less visible. If measurements were done more frequently, perhaps a similar pattern could be observed there as well.

The Hyltemossa data can also be compared with the field-observed global LAI database (Iio and Ito 2014) used and plotted by Parker (2020). Looking at the distribution of LAI for conifers, the most frequent values are between 3 and 4 (15% of all LAI values), 4-5 (17%) and 5-6 (12%) while values of 2-3, and 6-9 are less common, but still found in good numbers. The LAI calculated for Hyltemossa has an average between 4 and 5, meaning that it falls under the most common category.

6 Conclusion.

Looking back at the aims and research questions, not all the research questions can be answered. Regarding the variation of **k**, it varies substantially for the different weather conditions and the value for clear weather shows a seasonal pattern, decreasing during summer.

Calculated LAI followed the main pattern of the measured discontinuous values rather well, and while there were many outliers, the average values of 4-5 were in a similar range.

The apparent changes in LAI could be the result of the high standard deviation, and as such, it is difficult to say whether the changes in LAI caused by plant stress are visible in the data or not. Thus, detecting such stress events from the LAI data alone does not seem to be possible.

7 References.

Bendavid, N. S., H. D. Alexander, S. P. Davydov, H. Kropp, M. C. Mack, S. M. Natali, S. A. Spawn-Lee, N. S. Zimov, et al. 2023. Shrubs Compensate for Tree Leaf Area Variation and Influence Vegetation Indices in Post-Fire Siberian Larch Forests. *Journal of Geophysical Research: Biogeosciences*, 128**:** e2022JG007107. DOI: https://doi.org/10.1029/2022JG007107

Biermann, T., M. Heliasz, J. Holst, T. Holst, M.-L. Linderson, M. Mölder, J. Rinne, and I. Sweden. 2020a. Ecosystem eco time series (ICOS Sweden), Hyltemossa, 2018-12-31–2019-12-31. ICOS Sweden.

Biermann, T., M. Heliasz, J. Holst, T. Holst, M.-L. Linderson, M. Mölder, J. Rinne, and I. Sweden. 2020b. Ecosystem meteo time series (ICOS Sweden), Hyltemossa, 2018-12-31–2019-12-31. ICOS Sweden.

Biermann, T., M. Heliasz, J. Holst, T. Holst, M.-L. Linderson, M. Mölder, J. Rinne, and I. Sweden. 2021a. Ecosystem eco time series (ICOS Sweden), Hyltemossa, 2019-12-31–2020-12-31. ICOS Sweden.

Biermann, T., M. Heliasz, J. Holst, T. Holst, M.-L. Linderson, M. Mölder, J. Rinne, and I. Sweden. 2021b. Ecosystem meteo time series (ICOS Sweden), Hyltemossa, 2019-12-31–2020-12-31. ICOS Sweden.

Biermann, T., M. Heliasz, J. Holst, T. Holst, M.-L. Linderson, M. Mölder, and I. Sweden. 2020c. Ecosystem eco time series (ICOS Sweden), Hyltemossa, 2017-12-31–2018-12-31. ICOS Sweden.

Biermann, T., M. Heliasz, J. Holst, T. Holst, M.-L. Linderson, M. Mölder, and I. Sweden. 2020d. Ecosystem meteo time series (ICOS Sweden), Hyltemossa, 2017-12-31–2018-12-31. ICOS Sweden.

Chen, J. M., and T. A. Black. 1992. Defining leaf area index for non-flat leaves. *Plant Cell and Environment*, 15**:** 421-429.

Chen, J. M., and J. Cihlar. 1996. Retrieving leaf area index of boreal conifer forests using Landsat TM images. *Remote Sensing of Environment*, 55**:** 153-162. DOI: https://doi.org/10.1016/0034-4257(95)00195-6

Chen, J. M., P. M. Rich, S. T. Gower, J. M. Norman, and S. Plummer. 1997. Leaf area index of boreal forests: Theory, techniques, and measurements. *Journal of Geophysical Research: Atmospheres*, 102**:** 29429-29443. DOI: https://doi.org/10.1029/97JD01107

Gonsamo, A., and J. M. Chen. 2014. Continuous observation of leaf area index at Fluxnet-Canada sites. *Agricultural and Forest Meteorology*, 189-190**:** 168-174. DOI: https://doi.org/10.1016/j.agrformet.2014.01.016

Heliasz, M., N. Kljun, T. Biermann, J. Holst, T. Holst, M.-L. Linderson, M. Mölder, and J. Rinne. 2022. ETC L2 Meteosens, Hyltemossa, 2017-12-31–2022-08-31. Ecosystem Thematic Centre.

Heliasz, M., N. Kljun, T. Biermann, J. Holst, T. Holst, and M. Mölder. 2023. ETC NRT Meteosens, Hyltemossa, 2022-08-31–2023-03-15. Ecosystem Thematic Centre.

Hojas Gascón, L., G. Ceccherini, F. J. García Haro, V. Avitabile, and H. Eva. 2019. The Potential of High Resolution (5 m) RapidEye Optical Data to Estimate Above Ground Biomass at the National Level over Tanzania. *Forests*, 10**:** 107.

Holst, T., S. Hauser, A. Kirchgäßner, A. Matzarakis, H. Mayer, and D. Schindler. 2004. Measuring and modelling plant area index in beech stands. *International Journal of Biometeorology*, 48**:** 192-201. DOI: 10.1007/s00484-004-0201-y

Hutchison, B. A., and D. R. Matt. 1977. The annual cycle of solar radiation in a deciduous forest. *Agricultural Meteorology*, 18**:** 255-265. DOI: https://doi.org/10.1016/0002-1571(77)90017-6

ICOS-Sweden. 2023. Hyltemossa. Retrieved, from https://www.icos-sweden.se/hyltemossa.

Iio, A., and A. Ito. 2014. A Global Database of Field-observed Leaf Area Index in Woody Plant Species, 1932-2011. ORNL Distributed Active Archive Center.

Jonckheere, I., S. Fleck, K. Nackaerts, B. Muys, P. Coppin, M. Weiss, and F. Baret. 2004. Review of methods for in situ leaf area index determination: Part I. Theories, sensors and hemispherical photography. *Agricultural and Forest Meteorology,* 121**:** 19-35. DOI: https://doi.org/10.1016/j.agrformet.2003.08.027

Kalogirou, S. A. 2012. Solar thermal systems: Components and applications - introduction.

Li, D., X. Gu, Y. Pang, B. Chen, and L. Liu. 2018. Estimation of Forest Aboveground Biomass and Leaf Area Index Based on Digital Aerial Photograph Data in Northeast China. *Forests,* 9**:** 275.

Liang, S., and J. Wang. 2020. Chapter 10 - Leaf area index. In *Advanced Remote Sensing (Second Edition)*, eds. S. Liang, and J. Wang, 405-445. Academic Press.

Mencuccini, M., and L. Bonosi. 2001. Leaf/sapwood area ratios in Scots pine show acclimation across Europe. *Canadian Journal of Forest Research,* 31**:** 442-456. DOI: 10.1139/cjfr-31-3-442

Nassar, A., A. F. Torres-Rua, W. P. Kustas, H. Nieto, M. McKee, L. E. Hipps, D. Stevens, J. G. Alfieri, et al. 2020. Influence of Model Grid Size on the Estimation of Surface Fluxes Using the Two Source Energy Balance Model and sUAS Imagery in Vineyards. *Remote sensing,* 12.

Parker, G. G. 2020. Tamm review: Leaf Area Index (LAI) is both a determinant and a consequence of important processes in vegetation canopies. *Forest Ecology and Management,* 477**:** 118496. DOI: https://doi.org/10.1016/j.foreco.2020.118496

Qiao, K., W. Zhu, Z. Xie, and P. Li (2019) Estimating the Seasonal Dynamics of the Leaf Area Index Using Piecewise LAI-VI Relationships Based on Phenophases. *Remote Sensing,* 11.

Qu, Y., J. Wang, J. Song, and J. Wang. 2017. Potential and Limits of Retrieving Conifer Leaf Area Index Using Smartphone-Based Method. *Forests,* 8**:** 217.

Ross, J. 1981. The radiation regime and architecture of plant stands. In *Tasks for vegetation sciences 3*.

Ryu, Y., J. Verfaillie, C. Macfarlane, H. Kobayashi, O. Sonnentag, R. Vargas, S. Ma, and D. D. Baldocchi. 2012. Continuous observation of tree leaf area index at ecosystem scale using upward-pointing digital cameras. *Remote Sensing of Environment,* 126**:** 116-125. DOI: https://doi.org/10.1016/j.rse.2012.08.027

Thimonier, A., I. Sedivy, and P. Schleppi. 2010. Estimating leaf area index in different types of mature forest stands in Switzerland: a comparison of methods. *European Journal of Forest Research,* 129**:** 543-562.

Wang, R., J. M. Chen, Z. Liu, and A. Arain. 2017. Evaluation of seasonal variations of remotely sensed leaf area index over five evergreen coniferous forests. *ISPRS Journal of Photogrammetry and Remote Sensing,* 130**:** 187-201. DOI: https://doi.org/10.1016/j.isprsjprs.2017.05.017

Watson, D. J. 1952. The Physiological Basis of Variation in Yield. In *Advances in Agronomy*, ed. A. G. Norman, 101-145. Academic Press.

Yan, G., R. Hu, J. Luo, M. Weiss, H. Jiang, X. Mu, D. Xie, and W. Zhang. 2019. Review of indirect optical measurements of leaf area index: Recent advances, challenges, and perspectives. *Agricultural and Forest Meteorology,* 265**:** 390-411. DOI: https://doi.org/10.1016/j.agrformet.2018.11.033

8 Supplementary materials.

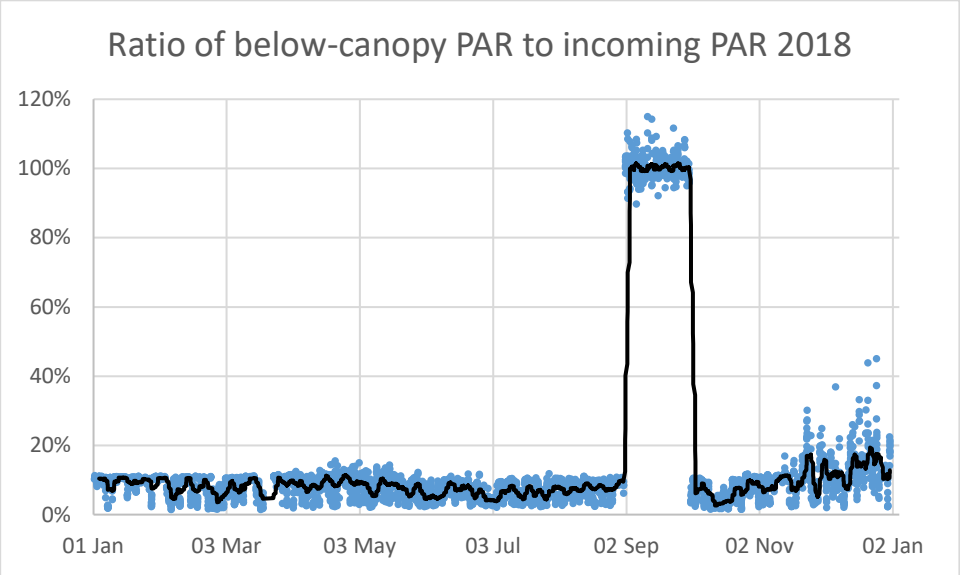

Figure S1. Ratio of below-canopy PAR to incoming PAR. Blue dots: individual values, black line: moving average over three days.

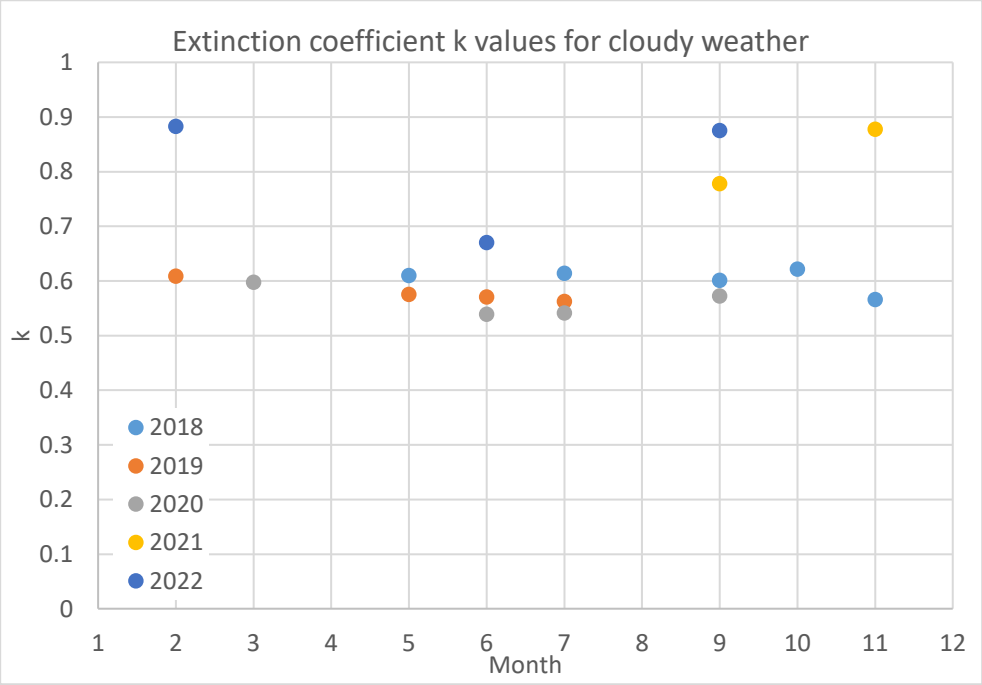

Figure S2. Values of k (extinction coefficient) for cloudy weather each month of measurement 2018-2022.

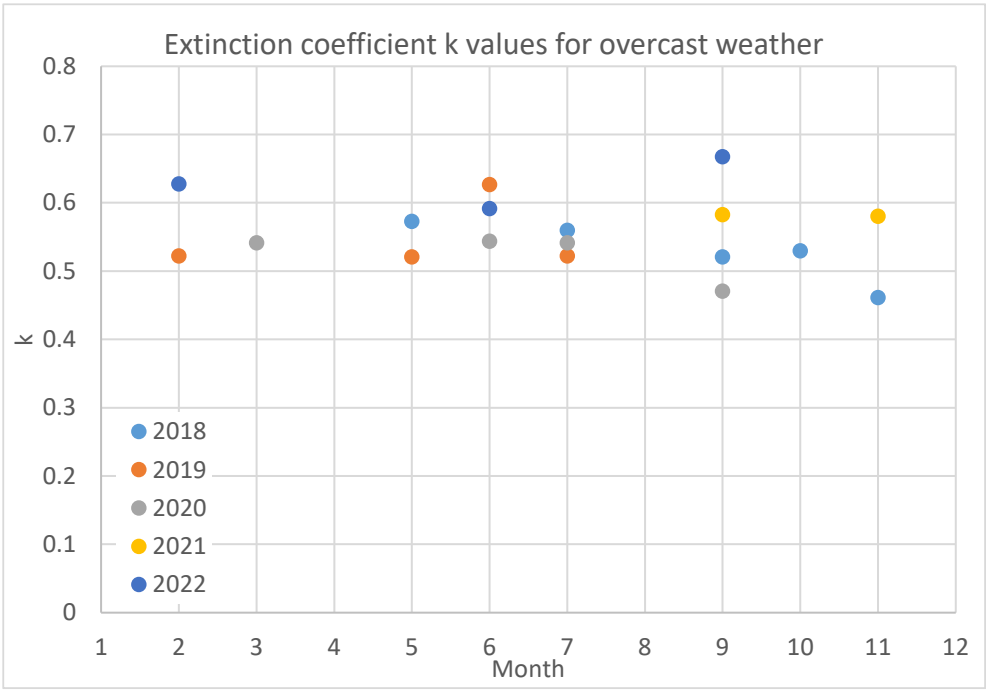

Figure S3. Values of k (extinction coefficient) for overcast weather each month of measurement 2018-2022.

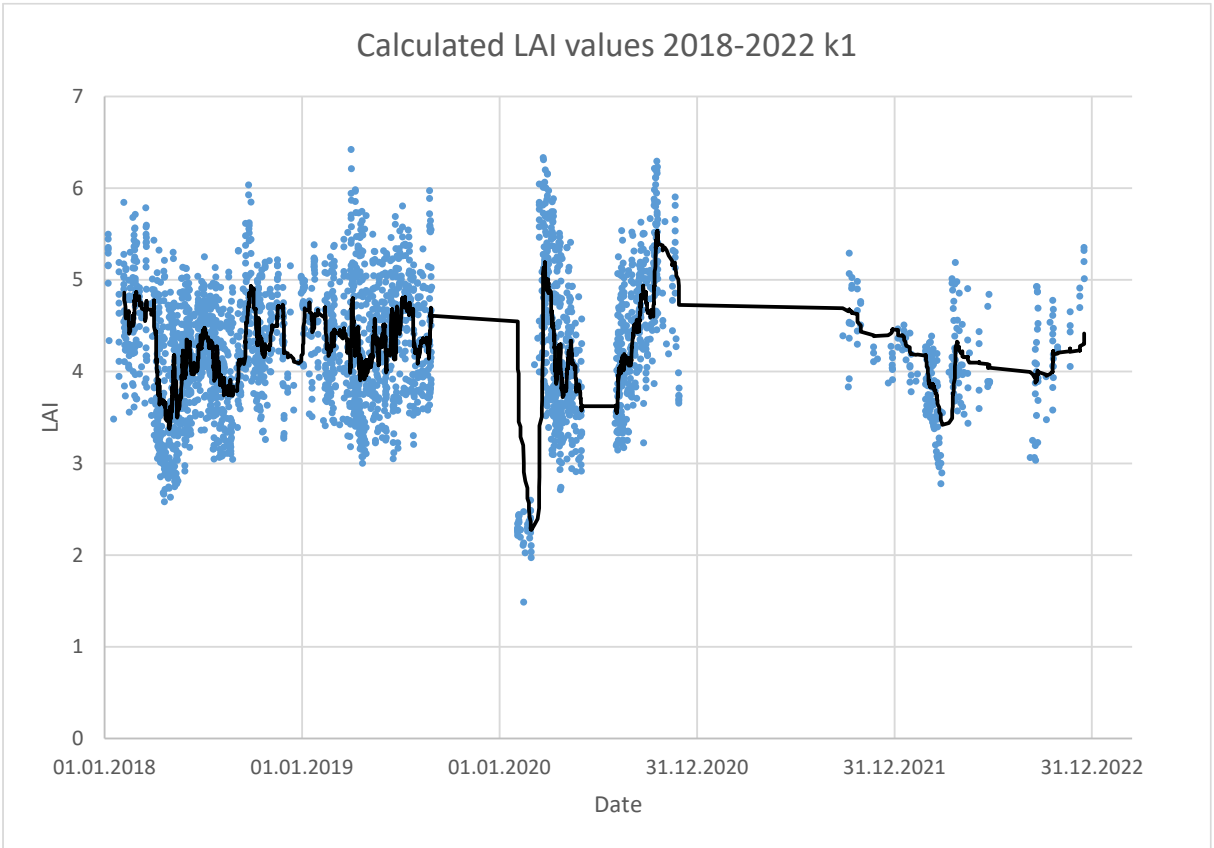

Figure S4. Calculated values of LAI for the entire five-year period for clear weather conditions. Blue dots: individual 30-min values during 10:00 – 14:00, black line: moving average over three days.

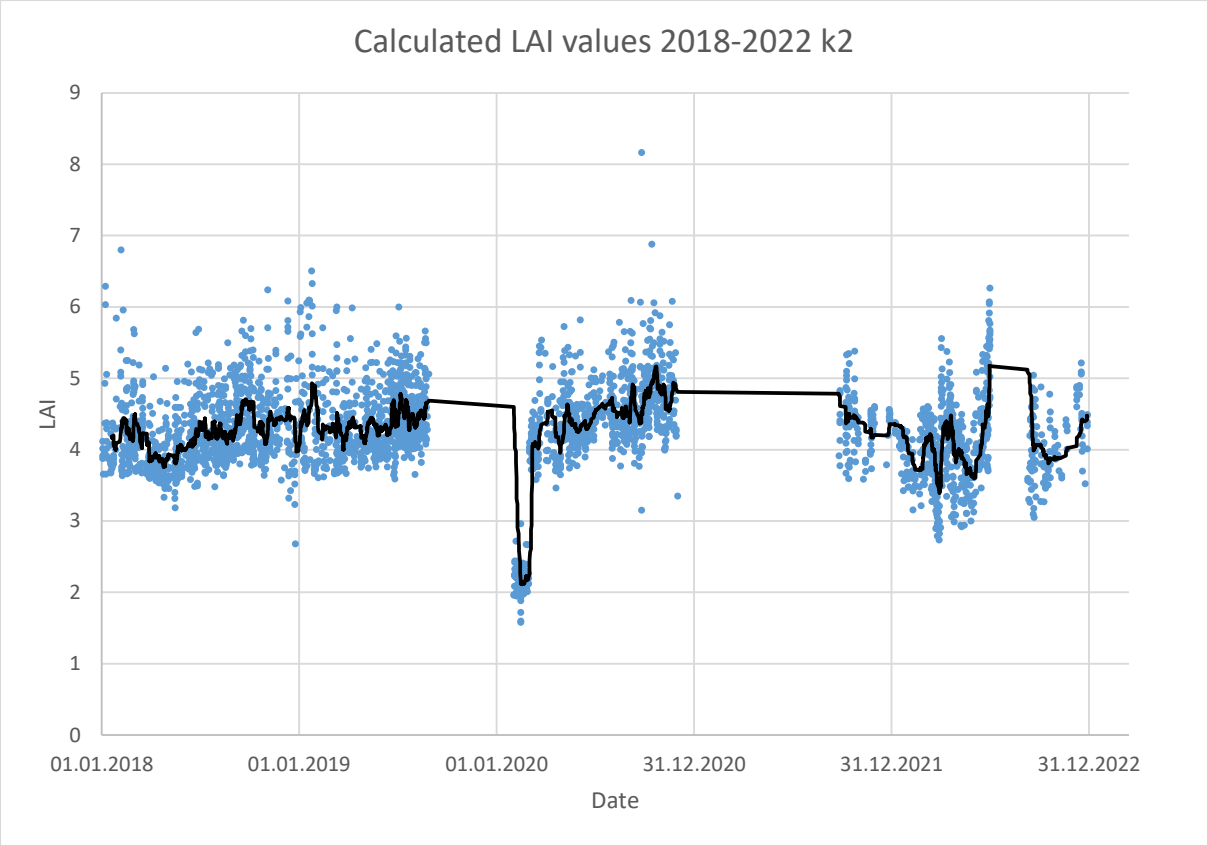

Figure S5. Calculated values of LAI for the entire five-year period for cloudy weather conditions. Blue dots: individual 30-min values during 10:00 – 14:00, black line: moving average over three days.

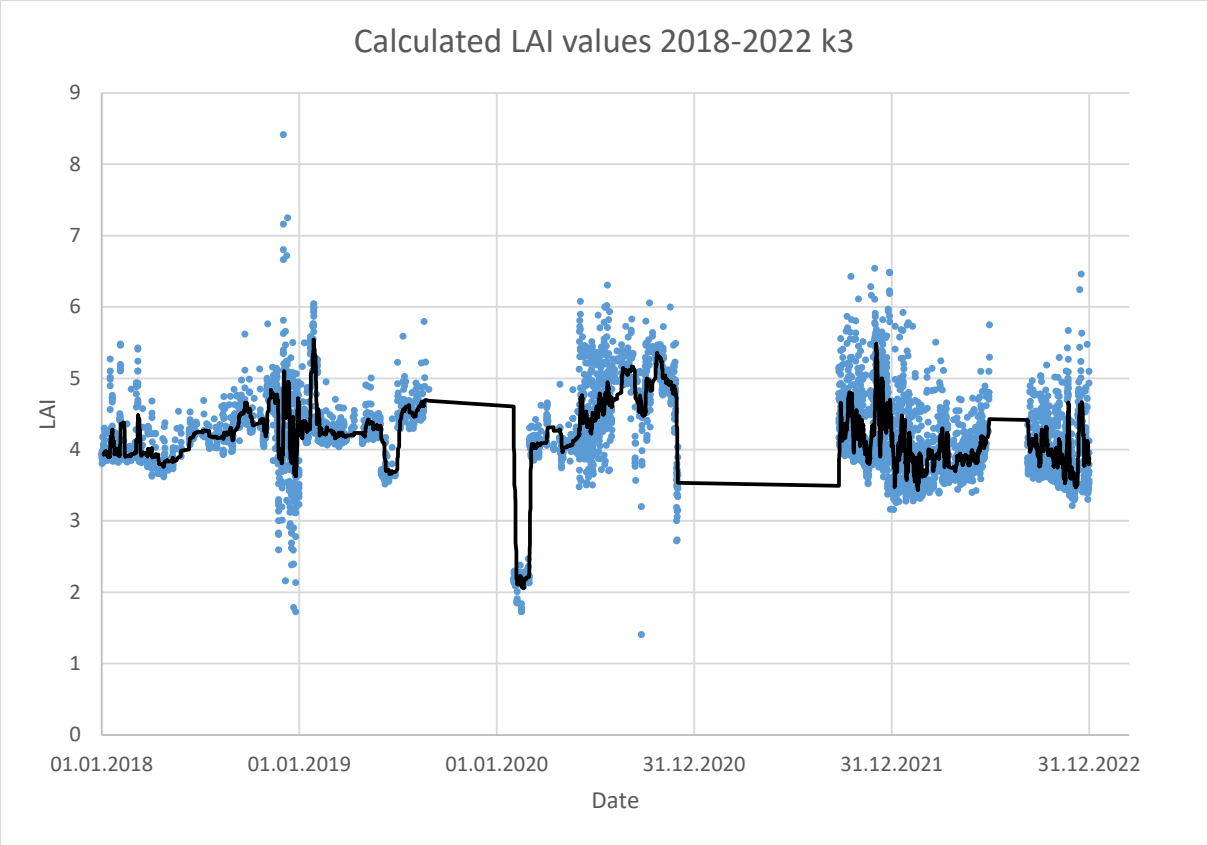

Figure S6. Calculated values of LAI for the entire five-year period for overcast weather conditions. Blue dots: individual 30-min values during 10:00 – 14:00, black line: moving average over three days.